AGU ADVANCING EARTH AND SPACE SCIENCES

Earth's Future

RESEARCH ARTICLE
10.1029/2024EF004661

Vegetation Greening Mitigates the Impacts of Increasing Extreme Rainfall on Runoff Events

Darren L. Ficklin[1], Danielle Touma[2], Benjamin I. Cook[3,4], Scott M. Robeson[1], Taehee Hwang[1], Jacob Scheff[5], A. Park Williams[6], Harper Watson[1], Ben Livneh[7,8], Mari R. Tye[9,10], and Lixin Wang[11]

[1]Department of Geography, Indiana University, Bloomington, IN, USA, [2]University of Texas Institute for Geophysics, University of Texas at Austin, Austin, TX, USA, [3]NASA Goddard Institute for Space Studies, New York, NY, USA, [4]Lamont-Doherty Earth Observatory, Palisades, NY, USA, [5]Department of Earth, Environmental and Geographical Sciences, University of North Carolina Charlotte, Charlotte, NC, USA, [6]Department of Geography, University of California, Los Angeles, CA, USA, [7]Cooperative Institute for Research in Environmental Sciences, University of Colorado Boulder, Boulder, CO, USA, [8]Civil, Environmental and Architectural Engineering, University of Colorado Boulder, Boulder, CO, USA, [9]NSF National Center for Atmospheric Research, Boulder, CO, USA, [10]Whiting School of Engineering, Johns Hopkins University, Baltimore, MD, USA, [11]Department of Earth and Environmental Sciences, Indiana University Indianapolis, Indianapolis, IN, USA

Key Points:

- The number and magnitude of extreme rainfall events are projected to increase throughout the global land surface
- Projected declines in event-based runoff ratio are found for a majority of the global land surface
- Projected runoff ratio declines are linked to decreased antecedent soil water from changes in individual evapotranspiration components

Supporting Information:

Supporting Information may be found in the online version of this article.

Correspondence to:

D. L. Ficklin,
dficklin@iu.edu

Citation:

Ficklin, D. L., Touma, D., Cook, B. I., Robeson, S. M., Hwang, T., Scheff, J., et al. (2024). Vegetation greening mitigates the impacts of increasing extreme rainfall on runoff events. *Earth's Future*, *12*, e2024EF004661. https://doi.org/10.1029/2024EF004661

Received 15 MAR 2024
Accepted 26 SEP 2024

Author Contributions:

Conceptualization: Darren L. Ficklin, Danielle Touma, Benjamin I. Cook, Scott M. Robeson, Taehee Hwang, Jacob Scheff, A. Park Williams, Lixin Wang
Data curation: Harper Watson
Formal analysis: Darren L. Ficklin
Investigation: Taehee Hwang
Methodology: Darren L. Ficklin, Danielle Touma, Benjamin I. Cook, Scott M. Robeson, Taehee Hwang, Jacob Scheff, A. Park Williams, Ben Livneh, Lixin Wang
Resources: Danielle Touma
Software: Darren L. Ficklin, Scott M. Robeson
Validation: Mari R. Tye
Visualization: Darren L. Ficklin, Danielle Touma, Benjamin I. Cook, Scott M. Robeson, Jacob Scheff,

Abstract Future flood risk assessment has primarily focused on heavy rainfall as the main driver, with the assumption that projected increases in extreme rain events will lead to subsequent flooding. However, the presence of and changes in vegetation have long been known to influence the relationship between rainfall and runoff. Here, we extract historical (1850–1880) and projected (2070–2100) daily extreme rainfall events, the corresponding runoff, and antecedent conditions simulated in a prominent large Earth system model ensemble to examine the shifting extreme rainfall and runoff relationship. Even with widespread projected increases in the magnitude (78% of the land surface) and number (72%) of extreme rainfall events, we find projected declines in event-based runoff ratio (runoff/rainfall) for a majority (57%) of the Earth surface. Runoff ratio declines are linked with decreases in antecedent soil water driven by greater transpiration and canopy evaporation (both linked to vegetation greening) compared to areas with runoff ratio increases. Using a machine learning regression tree approach, we find that changes in canopy evaporation is the most important variable related to changes in antecedent soil water content in areas of decreased runoff ratios (with minimal changes in antecedent rainfall) while antecedent ground evaporation is the most important variable in areas of increased runoff ratios. Our results suggest that simulated interactions between vegetation greening, increasing evaporative demand, and antecedent soil drying are projected to diminish runoff associated with extreme rainfall events, with important implications for society.

Plain Language Summary Climate change is leading to increases in the magnitude and number of extreme rainfall events. These increases in extreme rainfall events are often assumed to lead to an increase in extreme flooding events. However, using a climate model ensemble, our results indicate that changes in vegetation and atmospheric water demand may alter the relationship between extreme rainfall and extreme runoff. Notably, for a majority of the Earth surface, we find that projected changes in atmospheric aridity and vegetation lead to drier soil conditions prior to the extreme rainfall event that reduces the amount of hydrologic runoff generated. These findings have important implications for water resources management.

1. Introduction

Hydrologic extremes have severe consequences for human, environmental, and economic sectors. One of the well-established outcomes of ongoing climate change is an increase in the number and magnitude of extreme precipitation events even with minimal changes in annual or seasonal precipitation (Kirchmeier-Young & Zhang, 2020; Pendergrass & Knutti, 2018; Polson et al., 2013). Even for areas that are projected to experience a decline in annual precipitation, the number and intensity of short duration heavy precipitation events are likely to increase (Allan et al., 2021). This increase in precipitation extremes has already been observed throughout the world (Barbero et al., 2017; Westra et al., 2013), with sub-daily extreme precipitation changes generally aligning at or above the Clausius-Clapeyron relationship (~7%°C^{-1}; Visser et al., 2021) and a lower precipitation sensitivity (2%–3%°C^{-1}) for longer time intervals due to energetic constraints (Allen & Ingram, 2002; Visser

A. Park Williams, Ben Livneh, Lixin Wang
Writing – original draft: Darren L. Ficklin, Danielle Touma, Benjamin I. Cook, Scott M. Robeson, Taehee Hwang, Jacob Scheff, A. Park Williams, Ben Livneh, Mari R. Tye, Lixin Wang
Writing – review & editing: Darren L. Ficklin, Danielle Touma, Benjamin I. Cook, Scott M. Robeson, Taehee Hwang, Jacob Scheff, A. Park Williams, Ben Livneh, Lixin Wang

et al., 2021). Climate model projections agree with these observations and suggest that precipitation extremes will continue to increase into the future with increases in air temperature (Ficklin et al., 2022; Visser et al., 2021) with high confidence (Allan et al., 2021).

It is often assumed that extreme precipitation increases also will lead to increases in extreme runoff. However, previous work has suggested that this is not always the case (Ivancic & Shaw, 2015; Sharma et al., 2018; Wasko et al., 2021; Zhang et al., 2022), resulting in uncertain regional runoff and subsequent flooding trends under increasing extreme precipitation (Blöschl et al., 2019; Mallakpour & Villarini, 2015; Wasko & Nathan, 2019; Wasko et al., 2021; Zhang et al., 2022). Prior work suggests that these discrepancies might stem from changes in the extreme runoff generation mechanisms, where increases in rain-induced extreme runoff events are offset by decreases in snowmelt-induced extreme runoff events (Burn & Whitfield, 2023; Zhang et al., 2022). However, there remains a lack of consensus of runoff trends from extreme precipitation events (Mallakpour & Villarini, 2015; Wasko et al., 2021), suggesting that (a) we lack a thorough understanding of how the interaction between climate and biotic factors affect precipitation partitioning into runoff and soil-water infiltration, and (b) mechanistic drivers of the changes in antecedent conditions need to be examined in more detail. Additionally, given that extreme runoff events in many colder climates are transitioning from snowmelt-to rain-driven (Burn & Whitfield, 2023; Zhang et al., 2022), we need an improved understanding of the relationship between future extreme precipitation and runoff in multiple environmental and climatic settings.

Antecedent soil water content is the largest modulator of the amount of runoff from precipitation (Berghuijs et al., 2019; Ivancic & Shaw, 2015; Wasko & Nathan, 2019). With climate change, declines in surface-layer soil water content are expected, even with increases in precipitation (Cook et al., 2020; Stevenson et al., 2022), stemming from increases in vegetation water use due to greening (Li et al., 2023; Mankin et al., 2017, 2018, 2019) and atmospheric demand due to higher temperatures (Ficklin & Novick, 2017; Novick et al., 2016). Additionally, vegetation greening can increase canopy interception, which increases canopy evaporation and results in further declines in soil water content (Mankin et al., 2019). Much of this work, however, has been on the seasonal or annual scale, masking how these changes alter the event-based relationship between extreme precipitation and runoff that makes up a substantial portion of flooding events (Gillett et al., 2022). An increased understanding of this relationship is crucial for water resource and hazard planning.

Here, we address this knowledge gap by investigating the changing relationship between projected changes in daily extreme precipitation events (liquid precipitation; hereafter "rainfall") and the corresponding runoff. Specifically, we analyze daily rainfall and runoff from 30 members of the state-of-the-art Community Earth System Model version 2–Large Ensemble (CESM2-LE; Rodgers et al., 2021) under historical and projected medium-to-high scenario climate forcing (SSP3-7.0; Meinshausen et al., 2020). Using a large ensemble allows for robust sampling of extreme rainfall and runoff events while also controlling for radiative forcing and model uncertainty or biases (Mankin et al., 2020; Stevenson et al., 2022; Touma et al., 2021, 2022). Although data from multiple large ensembles are publicly available, only the CESM2-LE output provides relatively high temporal (daily) and spatial (~1°) resolutions, includes all the required variables needed for the analysis, and has a relatively large ensemble size (see Section 2).

2. Materials and Methods

2.1. Community Earth System Model Version 2–Large Ensemble

The Community Earth System Model (CESM) is a fully coupled, global-scale climate model with a grid resolution of 0.9424° latitude X 1.25° longitude. CESM uses the Community Land Model (CLM; Lawrence et al., 2019) to simulate land surface processes. We use individual members of the CESM2 Large Ensemble (CESM2-LE; Rodgers et al., 2021) to assess whether the probability of extreme runoff from extreme rainfall will change in the future. The CESM2-LE is a 100-member ensemble that was run from 1850 to 2014 under historical forcing and from 2015 to 2100 under the high-emission SSP3-7.0 scenario. We use the first 30 of these ensemble members, which allows us to balance computational time/effort for analyzing multiple global daily time series while also sufficiently capturing the impact of forced changes in climate variability on extreme rainfall and runoff events (Milinski et al., 2020). CLM simulates runoff using a combination of surface and subsurface runoff. Surface and subsurface runoff are derived from soil moisture (e.g., saturation, saturated thickness) and topographic characteristics (e.g., slope; Lawrence et al., 2019). Full details on the CESM2-LE model and initializations can be found in the model documentation (Danabasoglu et al., 2020; Rodgers et al., 2021).

10.1029/2024EF004661

From the CESM2-LE, we extracted simulated variables related to rainfall and runoff. Specifically, daily rainfall (specified as RAIN in the CESM2-LE model output naming convention), total runoff (QRUNOFF; a variable used in previous work; Scheff et al., 2022), and snow depth (SNOWDP; used to assess whether snow was present on the ground at the time of the extreme rainfall event). The extracted daily antecedent variables were liquid water in the top 10 cm of the soil (SOILWATER_10CM), transpiration (QVEGT), canopy evaporation (QVEGE), ground evaporation (QSOIL), total projected leaf area index (TLAI), and reference height (2 m) air temperature (TREFHT) and relative humidity (RHREFHT) used to calculate vapor pressure deficit (VPD).

2.2. Runoff Ratio and Antecedent Analyses

For each CESM2-LE member, we find the 95th percentile of rainfall and runoff (with dry days removed; defined as <0.01 mm) occurring on a snow-free surface for the pre-industrial historical (1850–1880) time period for each land surface grid cell. This time period was chosen to eliminate any influence of climate change on extreme precipitation, runoff, and antecedent conditions. Based on the aforementioned definitions, we then extract every rainfall event that meets or exceeds the historical 95th percentile of rainfall for the historical and projected (2070–2100) time periods that also occurs on a snow-free surface. For consecutive days with rainfall ≥95th percentile, the rainfall, runoff (day of or day after), and antecedent conditions corresponding to the first day are extracted. We chose days without a snowpack present to only assess the rainfall-runoff relationship and not include snowmelt from rain-on-snow as part of the runoff. For each extreme rainfall event, we then extract the maximum runoff from this event, which is defined as the maximum runoff on the day of or the day after the extreme rainfall event. The runoff ratio is estimated by dividing the maximum runoff depth by the extreme rainfall event depth. The probability of extreme runoff is estimated by dividing how many extreme runoff events occurred (based on its historical 95th percentile) by the total number of extreme rainfall events (# of extreme runoff events/# of extreme rainfall events).

To assess the state of the antecedent hydrologic conditions prior to the extreme rainfall event, we extract the antecedent variables (see above for CESM2 variable names) for each extreme rainfall event for the historical and projected time periods. Specifically, we examine surface-layer soil-water content (top 10 cm of the soil column), which is highly sensitive to runoff and ground evaporation (Penna et al., 2011), evapotranspiration (separated into its components: ground evaporation + canopy evaporation + plant transpiration), leaf area index (LAI), vapor-pressure deficit (VPD), and total rainfall prior to the extreme rainfall event. We examine surface-layer soil water content because the event-based runoff examined in this study is mostly driven by stormflow (rapid surface and subsurface flow) while baseflow levels (between rainfall events) are mainly influenced by deep soil and groundwater flow (Katsuyama et al., 2009; Penna et al., 2011; Scipal et al., 2005; Singh et al., 2021). To quantify the mean state of the antecedent conditions and to match up with rainfall, runoff, and runoff ratio (which are a singular value), we take the mean of each antecedent variable for the 5 days preceding the day of the extreme rainfall event (but does not include the day of the extreme rainfall event), a commonly used time period for rainfall-runoff analyses (NRCS, 2004) that also includes shorter-duration events. We acknowledge that the antecedent time period can vary depending on the time of year and location (Brocca et al., 2008; Mishra & Singh, 2006), and therefore we also compare the 5-day antecedent results with a longer antecedent time period (14 days) in the Supporting Information S1. Moreover, future climate projections often indicate a widespread occurrence of time-mean surface soil drying (Cook et al., 2020), suggesting that changes in antecedent soil water content may not be affected by the length of the antecedent time period. Finally, historical and projected time period results are summarized by taking the median of all extreme rainfall, runoff and their antecedent conditions for the entire time period, resulting in one value for each time period for extreme rainfall, runoff and the antecedent conditions (surface-layer soil-water content, evapotranspiration and its individual components, LAI, VPD, and total prior rainfall). This was done for each land surface grid cell and ensemble member ($n = 30$). Changes (either percent change or ratio change) are based on these values, and an CESM2-LE mean was calculated.

2.3. Statistical Analyses

To attribute changes between extreme rainfall, runoff and antecedent variables, we perform correlations and machine learning regression tree ensembles. Due to the variety of relationships between rainfall, runoff, and antecedent variables, we use Spearman's rank correlations (r_s). Additionally, due to the differential grid-box areas, r_s values are estimated using probability-weighted bootstrap sampling ($n = 1000$) and are presented as the mean of the bootstrapped correlations. Unless otherwise noted, these correlations were performed at the global

10.1029/2024EF004661

scale for all land surface grid cells (n – 14,000). While correlation analyses on their own do not indicate a causal relationship, they allow us to document the strength and direction of relationships between important variables.

To control for the influence of changing antecedent rainfall on antecedent conditions (specifically soil water content), we perform an additional analysis where we extract all land surface areas (or grid cells) with minimal changes in ensemble mean antecedent rainfall (±10%) from the historical to projected time periods. In addition to minimal changes in antecedent rainfall, areas with ensemble mean increases in runoff ratio (projected runoff ratio/historical runoff ratio > 1) and decreases (<1) are further extracted for analyses. This results in two spatial units (one with increases in runoff ratio and one with decreases) with a large number of grid cells that have minimal projected changes in antecedent rainfall. For these separated regions, we use the nonparametric Mood's median test to assess whether the medians are significantly different between regions of increasing and decreasing runoff ratio and minimal changes in antecedent rainfall.

For these separated regions, we also use a machine-learning regression-tree approach to understand how changes in individual antecedent evapotranspiration components (related to greening) are related to changes in antecedent soil water content, a dominant variable in determining the rainfall-runoff relationship (Penna et al., 2011). Specifically, the dependent variable is the ensemble mean change in antecedent soil water content from the historical to the projected time period, while the independent variables are changes in antecedent transpiration, canopy evaporation, ground evaporation, and total antecedent rainfall. This approach was performed separately for areas with increases and areas with decreases in the ensemble runoff ratio.

To understand the importance of the aforementioned variables in these separated regions, we use bagging (or bootstrap aggregation), a generalized version of a random forest approach. Rather than relying on an individual multiple regression model, bagging uses an ensemble of trees and aggregates results from each tree for a final model and prediction, resulting in reduced overfitting and improved generalization (Breiman, 1996, 2001). No distribution is assumed and the nonparametric fitting is flexible (James et al., 2013). From these individual regression models, the importance of independent variables (in this case, the antecedent variables) can be determined by calculating how much the objective function (in this case, mean square error) changes by swapping in and out the predictors and then dividing that value by the number of branches. This approach also accounts for correlations between predictor variables because at each step in the tree the best multiple predictors (in terms of the objective function) are selected.

With bagging, the number of bootstrapped samples (or number of trees to grow) must be defined. Then, for each tree, a minimum set of observations (or leaves) must also be defined for each tree branch. To find the number of trees to grow and minimum number of leaves, we examined the relationship between the mean square error and the number of trees and minimum number of leaves. The final values were chosen based on the number of trees and minimum number of leaves where model improvement leveled off. This results in a parsimonious model as possible to avoid overfitting. From this, we found that 15 number of trees with a minimum of 5 number of leaves were the optimal values. We used MATLAB® version 2021b to build the regression trees. More details about bagging in hydrology can be found in Zhang et al. (2018). We present model evaluation statistics for the regression tree ensemble model for both separated regions in Table S1 and Figure S1 of Supporting Information S1. Which antecedent variables are important for changes in antecedent soil water content for each region are presented in the results.

All calculations reported here use areal weighting or areal percentiles (Willmott et al., 2007), including the histograms summarizing the mapped results. When presenting our statistical results, we place a strong emphasis on effect size rather than significance tests, driven by the widespread recognition that significance testing should receive less attention (Gelman & Stern, 2006; Halsey, 2019).

2.4. Observational Comparisons

To ensure that the CESM2-LE is adequately simulating the relevant variables during the historical time period, we compare CESM2-LE outputs against multiple monthly gridded observations compiled by the International Land Model Benchmarking project (ILAMB; Collier et al., 2018; Table S2 in Supporting Information S1). These include runoff from the Conserving Land-Atmosphere Synthesis Suite (CLASS v1.1; Hobeichi et al., 2020) and Linear Optimal Runoff Aggregate (LORA v1.0; Hobeichi et al., 2019), surface soil moisture (Wang et al., 2021), evapotranspiration from the Global Land Evaporation Amsterdam Model (GLEAM; Martens et al., 2017) and

MOD16A2 (Mu et al., 2011), and LAI from MODIS (Myneni et al., 2002), AVHRR (Vermote, 2019), and AVH15C1 (Claverie et al., 2016). In addition to monthly comparisons, we also compare runoff from the CESM2-LE against runoff from the National Centers for Environmental Prediction/Department of Energy Reanalysis II (hereafter NCEP2; Kanamitsu et al., 2002a). Other relevant variables such as precipitation, temperature, and snowpack from the CESM2-LE have been validated in previous work (Abdelmoaty et al., 2021; Lawrence et al., 2019; McKinnon & Simpson, 2022; Wieder et al., 2022; Zeder & Fischer, 2024).

The validation data sets listed in Table S2 of Supporting Information S1 are linearly interpolated to the same spatial resolution as the CESM2-LE. Due to the lack of gridded, daily observations for all relevant variables, the CESM2-LE daily data are aggregated to a monthly time period for direct comparison with the monthly observations. While global submonthly observational data exists for some land surface and hydrological variables (e.g., MODIS ET), their temporal extents are relatively short, which impedes our ability to robustly assess submonthly uncertainties. Over such a short period of analysis, differences between CESM2-LE and the observational data sets could be dominated by differences in the phases of modes of variability like El Niño–Southern Oscillation (ENSO) or the Pacific Decadal Oscillation (PDO) and periods of accelerated warming, clouding our insight into the model uncertainties.

Between the CESM2-LE ensemble mean and gridded observations, we compare spatial biases in the mean state and the variability (using the interquartile range; IQR) of all months (January through December) during the direct time period overlap; see Table S2 in Supporting Information S1. For the mean and IQR, spatial biases are calculated by subtracting the observations from the CESM2-LE ensemble mean. Area-weighted Pearson correlations, area-weighted mean absolute errors, and kernel density scatterplots are calculated between the observations and the CESM2-LE ensemble mean. Using the overlapping monthly time series of the CESM2-LE ensemble mean and the observations, we also present the mean absolute error for each grid cell. Additionally, using the Theil-Sen trend test, we assess trends in greening between the CESM2-LE ensemble mean and LAI data sets in Table S2 of Supporting Information S1. For the NCEP2 daily runoff validation, we compared the 95th and 99th percentiles of runoff for the 1980–2009 overlapping time period for each data set. Results from these analyses are shown in Figures S2–S16, and Tables S2 and S3 of Supporting Information S1).

2.5. CMIP6 Monthly Comparisons

To ensure that the CESM2-LE projections are consistent with other CMIP6 models, we compare monthly projections of surface soil moisture (CMIP6 variable ID *mrsos*), runoff (*mrro*), evapotranspiration (evspsbl), and LAI (lai). Historical and projected (SSP3-7.0) CMIP6 data are downloaded from the Center for Environmental Data Analysis (CEDA) Archive (https://data.ceda.ac.uk/badc/cmip6/data) and are listed in Table S4 of Supporting Information S1. Daily data are not available for a large number of GCMs, so we assess the CESM2-LE projections using monthly data (the CESM2-LE daily data are aggregated to monthly data). All GCM data are linearly interpolated to the same spatial resolution of the CESM2-LE (0.9424° latitude X 1.25° longitude). Although this monthly comparison allows us to contextualize the overall spatial patterns of hydrologic and land surface variables in CESM2-LE, sufficient daily data availability for other CMIP6 models would have allowed for more relevant comparisons for our study. Using similar metrics as the CESM2-LE analysis, we compare changes from the historical to the projected time period. Results from this analysis are shown in Figures S17–S20, and Table S4 of Supporting Information S1).

3. Results and Discussion

3.1. Changes in Extreme Rainfall and Corresponding Runoff

The CESM2-LE projects widespread projected increases in both the magnitude and number of extreme rainfall events, consistent with previous work (Akinsanola et al., 2020; Pendergrass & Knutti, 2018). Figure S21 in Supporting Information S1 displays the CESM2-LE ensemble mean of the number of extreme rainfall events assessed for the historical and projected time periods. On average, the number of extreme rainfall events and their magnitudes increased across the land surface relative to the historical time period, with robust agreement among CESM2-LE members (defined as an agreement on the sign of the change for 2/3 of the ensemble members; Figures 1a and 1b). The largest percent increases in the numbers of extreme rainfall events were found in the northern hemisphere, with large changes in western North America, and western Asia (ensemble mean >150% increase), while portions of Central America, South America, the Mediterranean, and Africa showed slight

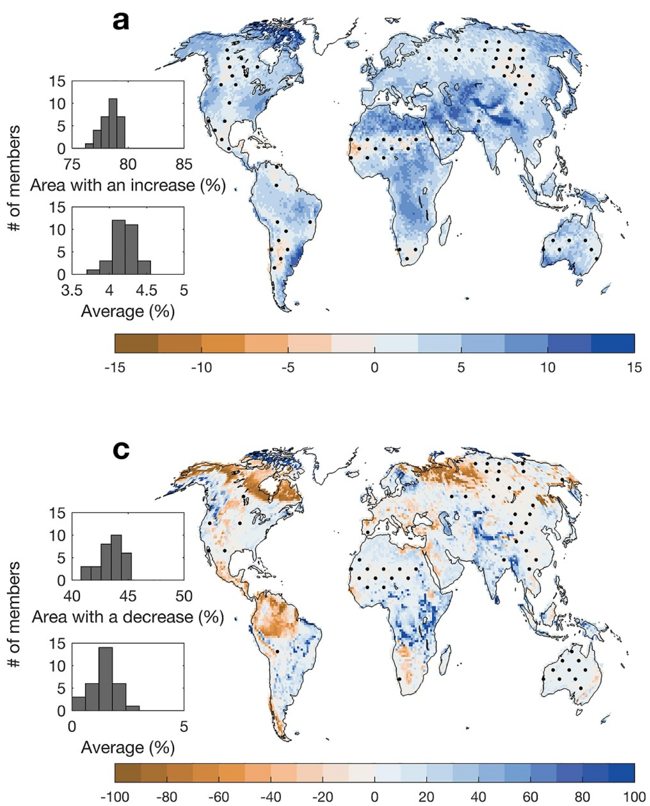

Figure 1. Ensemble mean of projected (2070–2100) changes from the historical time period (1850–1880) for (a) extreme rainfall magnitude (%), (b) number of extreme rainfall events (%), (c) probability of an extreme runoff event occurring from an extreme rainfall event (%), and (d) change in the event-based runoff ratio (projected/historical). The stippling indicates a non-robust ensemble agreement (defined as <2/3 of the ensemble members agree on the sign of the change). The histograms for each subpanel show the distribution of percent of the land surface with an increase (for a, b) or a decrease (for c, d) in the projections across the individual CESM2 members and the distribution of area-weighted land surface averages across the ensemble.

decreases (~10%–20%). Similarly, we found increases in extreme rainfall magnitude using the CESM2-LE ensemble mean, with large (>10%) increases found throughout the global land surface. In general, changes in the numbers of extreme rainfall events were much larger than those in the extreme rainfall magnitude (Figures 1a and 1b), likely due to energy limitations (Barbero et al., 2019; Ivancic & Shaw, 2015). In addition to the increases in extreme rainfall magnitude, the number of extreme rainfall events is projected to increase due to warming-driven transitions from snow to rain (number of historical and projected events shown in Figure S21 of Supporting Information S1). With a declining snowpack, more rainfall events also occur on a snow-free land surface (Musselman et al., 2018; Wieder et al., 2022). We recognize that the interpretation of an extreme precipitation event can vary between studies (Pendergrass, 2018). The 95th percentile used in this study allows for a robust sampling of rainfall-runoff events compared to events farther into the upper tail. We do, however, compare the runoff ratio using the 99th percentile as a threshold and found no substantial differences (Figures S22 and S23 in Supporting Information S1).

While we find increases in ensemble mean rainfall extremes for much of the land surface, these increases do not lead to concomitant increases in runoff extremes simulated by the CESM2-LE. We see declines in both the probability of extreme runoff and the event-based runoff ratio (projected runoff ratio/historical runoff ratio < 1) for 43.5% and 56.9% of the land surface, respectively, for the CESM2-LE ensemble mean (Figures 1c and 1d), with declines in the runoff ratio more widespread than declines in runoff magnitudes (Figure S24 in Supporting Information S1). There is widespread robust agreement among CESM2-LE members for the widespread declines in the runoff ratio, suggesting that declines in extreme runoff occur in the same places where extreme rainfall is projected to increase. While many of the grid points are near the runoff ratio increase/decrease division line (projected runoff ratio/historical runoff ratio = 1), it is important to note that these minor runoff ratio decreases are occurring even with a corresponding increase in extreme rainfall in both magnitude and number of events

10.1029/2024EF004661

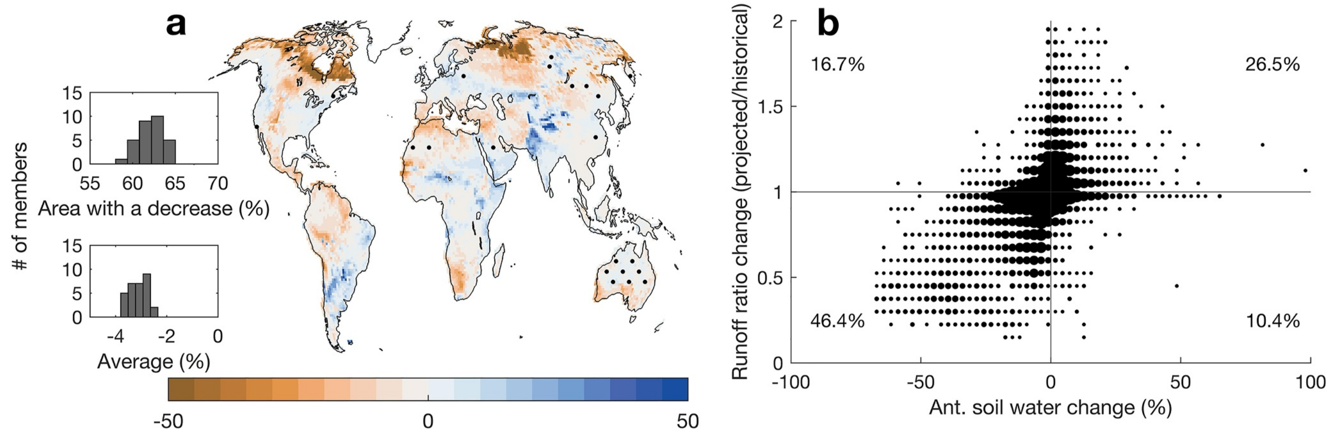

Figure 2. Ensemble mean of projected (2070–2100) changes from the historical time period (1850–1880) for (a) % change in antecedent surface soil water content and (b) a binned scatterplot of the relationship between changes in event runoff ratio and antecedent soil water for each land grid cell. The histograms in panel a show the projections from each individual member of the CESM2 large ensemble of area with a decrease and the area-weighted land surface average. The stippling indicates a non-robust ensemble agreement (defined as <2/3 of the ensemble members agree on the sign of the change). The size of the filled circles in b is proportional to the area of the terrestrial surface in each bin. The percentages in b represent the percent of the total area in each quadrant.

(Figure 1). Of the land surface area with a CESM2-LE ensemble mean projected runoff ratio decrease, 93% had an increase in extreme rainfall magnitude. This suggests that there are other mechanisms that account for these declines (or lack of increase).

These declines in event-based runoff ratio are largely concentrated in the northern high latitudes and Amazon region; however, we also find declines for portions of western North America and Central America (Figures 1c and 1d). Large increases in runoff ratio following extreme rainfall events are found in central Africa and western Asia (Figures 1c and 1d). We also find a weak correlation (area-weighted Spearman correlation $r_s = 0.31$) between changes in extreme rainfall magnitude and extreme runoff magnitude across all land grid cells ($n - 14{,}000$) in the ensemble mean field.

3.2. Drivers of Runoff Ratio Changes

We observe that areas with projected declines in event-based CESM2-LE simulated runoff ratios are linked to reduced antecedent soil water content ($r_s = 0.56$), even in locations experiencing increases in rainfall extremes (Figures 2a and 2b) and with an extended antecedent time period of 14 days (see Figure S25 in Supporting Information S1). Previous studies have also highlighted that this contrasting relationship under historical and projected changes in climate is largely controlled by simulated changes in antecedent soil water conditions (Ivancic & Shaw, 2015; Sharma et al., 2018; Wasko et al., 2021), particularly for frequent rainfall extremes where the rainfall rate does not exceed the top soil layer maximum infiltration rate (Masson-Delmotte et al., 2021). Building on this, we find widespread, robust declines in CESM2-LE ensemble mean antecedent soil water content for the land surface (ensemble average decline for 62% of land surface area; Figure 2a). The largest declines (−40% or less) are found in the northern latitudes, but other regions such as the western United States and the Amazon region also exhibit robust declines (−25% to −15%).

Antecedent rainfall (soil water increase) and the role of vegetation via transpiration and canopy evaporation (soil water decrease) are the dominant controls on antecedent soil water content (Jung et al., 2010) and therefore the runoff ratio. Antecedent soil water content has often been equated with antecedent rainfall (Woldemeskel & Sharma, 2016), but ongoing climate change increases evaporative and vegetation water demand, with sometimes rapid decreases in soil water content (Pendergrass et al., 2020; Yuan et al., 2023). Here, we find minimal changes in CESM2-LE simulated ensemble mean antecedent rainfall (ensemble average + 0.13%) with declines for 62% of the land surface area (Figure 3a), a further indication of hydrologic intensification whereby extreme events are preceded by drier than usual periods (Ficklin et al., 2022). The changes are spatially variable, with areas such as the Amazon region, western Africa, and western Asia exhibiting declines (−30% to −20%), while increases are found in regions such as western North America and portions of northern Africa and southern South America (25%–40%). It is also important to note that there are large areas (especially in the northern latitudes) where

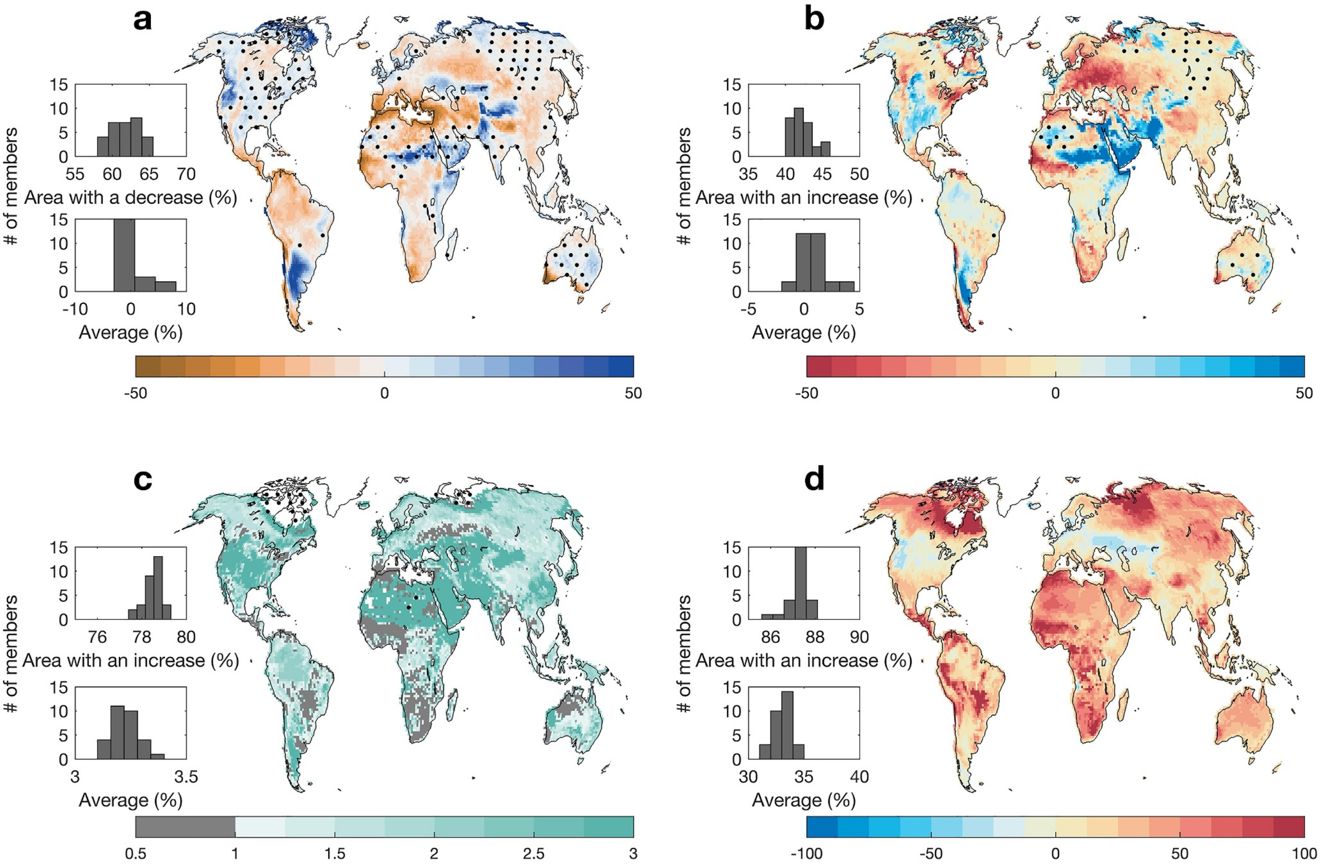

Figure 3. Ensemble mean of projected (2070–2100) changes from the historical time period (1850–1880) for (a) % changes in antecedent rainfall, (b) % changes in antecedent evapotranspiration, (c) change in antecedent leaf area index (LAI) (defined as projected antecedent LAI/historical antecedent LAI), and (d) % changes in antecedent vapor pressure deficit. The stippling indicates a non-robust ensemble agreement (defined as <2/3 of the ensemble members agree on the sign of the change). The histograms for each subpanel show the distribution of percent of the land surface with a decrease (for a) or an increase (for b–d) in the projections across the individual CESM2 members and the distribution of area-weighted land surface averages across the ensemble.

projected changes in antecedent rainfall are not robust. The Spearman correlation between changes in antecedent rainfall and antecedent soil water content is +0.42 for all land grid cells, suggesting that changes in antecedent rainfall exhibit some control on antecedent soil water content, but changes in evapotranspiration are likely important as well.

Overall, we find that the global land surface average simulated antecedent evapotranspiration increased by 0.67% for the projected time period, with increases found for 42.3% of the area (Figure 3b). There is an upper limit on how much evapotranspiration can occur, with some regions being water-limited or energy-limited or transitioning between these two regimes, resulting in high spatial variability of evapotranspiration and its relationship to soil water content (Berg & Sheffield, 2018). For example, Feng et al. (2023) found high spatial variability between the correlation of peak growing season soil moisture and evapotranspiration, with widespread areas having correlations of different signs. Additionally, using an ensemble of climate models, Berg and Sheffield (2018) found notable climate model diversity in global terrestrial soil moisture and evapotranspiration coupling in terms of both patterns and magnitude. Finally, Novick et al. (2016) found that VPD and soil moisture decouple as the temporal resolution increases (seasonal to hourly). While VPD is not the same as evapotranspiration, it is a large driver. Additionally, this work assesses correlations in percent changes from the historic to projected time periods in variables that are either at the daily time step (rainfall or runoff) or averages of the 5-day antecedent time period and then summarized for subsequent analyses. Both are snapshots in time, rather than an annual or seasonal time step where correlations between soil moisture and evapotranspiration are more coupled (Novick et al., 2016). It is not surprising, then, that the correlation between projected changes in antecedent soil water content and evapotranspiration for all land grid cells was weak ($r_s = 0.07$) and the correlation between changes in antecedent

10.1029/2024EF004661

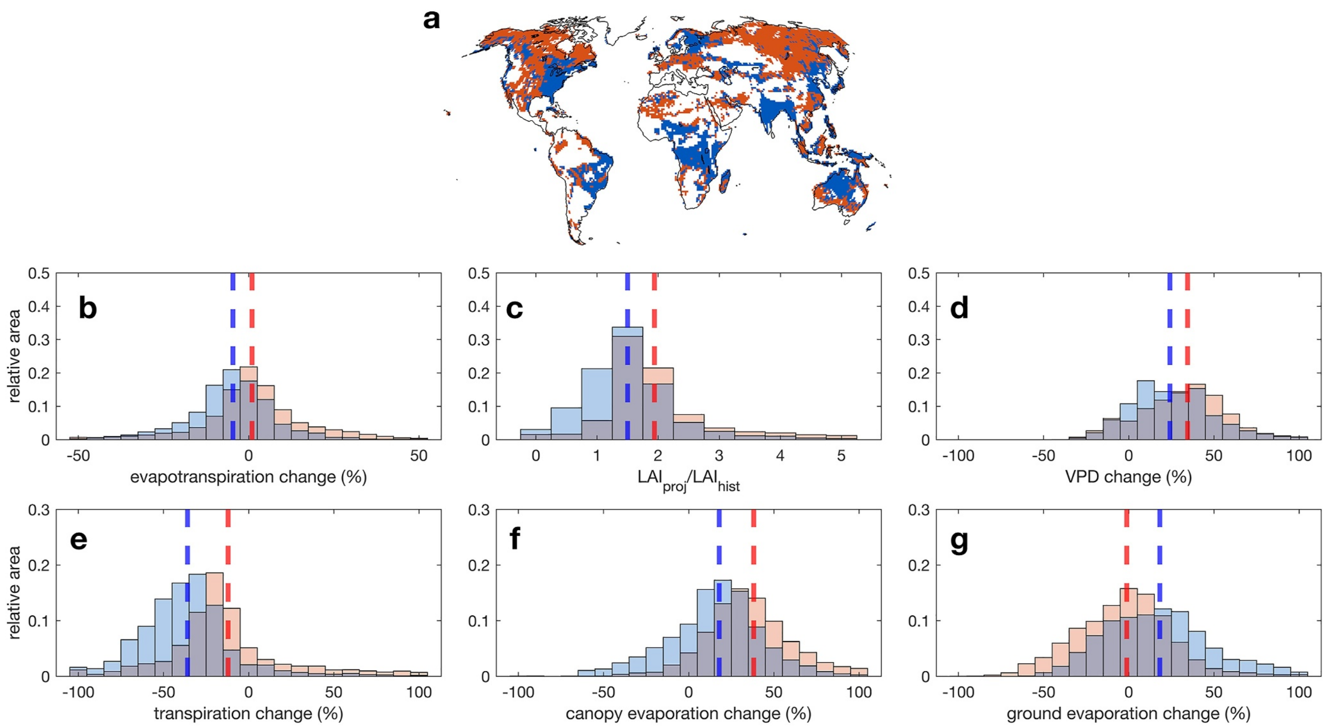

Figure 4. Summary of changes in antecedent conditions for areas with minimal projected antecedent rainfall change (±10%) but with increases or decreases in runoff ratio. The maps indicate the delineated areas for runoff ratio decreases (panel a; red color) and increases (panel a; blue color). The specific antecedent conditions assessed include evapotranspiration (b), leaf area index (LAI, defined as projected antecedent LAI/historical antecedent LAI; (c)), vapor pressure deficit VPD (d), transpiration (e), canopy evaporation (f), and ground evaporation (g). Vertical lines represent the area-weighted median for each grouping.

rainfall and evapotranspiration was moderate ($r_s = 0.30$). However, to instill confidence that the CESM2 ensemble is adequately simulating the coupling of evapotranspiration and surface soil moisture, we performed a Pearson correlation analysis between daily evapotranspiration and surface soil moisture (not just antecedent) from 1980 to 2009 and found strong coupling (both negative and positive) in energy- and water-limiting areas throughout the global land surface (Figure S26 in Supporting Information S1).

3.3. A Closer Look at Antecedent Conditions

Extreme rainfall events can be preceded by smaller antecedent rainfall events that replenish soil water content and alter evapotranspiration, resulting in changes to the runoff ratio. To address this, we perform an additional analysis separating areas where the CESM2-LE ensemble mean projected runoff ratio increases (projected runoff ratio/historical runoff ratio > 1) or decreases (ratio < 1). Within these separated areas, we also extract areas where antecedent rainfall changes minimally (±10%) compared to the historical time period, thus allowing for a consistent comparison of antecedent soil water content inputs (i.e., rainfall) between the historical and projected time periods. Taken together, this allows for a comparison of changes in the runoff ratio while controlling for changes in antecedent rainfall. Using these separation thresholds, we find that runoff ratio increases for 28% of the land surface (excluding Greenland and Antarctica) and decreases for 30% of the land surface, while controlling for minimal changes in antecedent rainfall. Diverse environments are represented in each category (Figure 4a).

After controlling for changes in antecedent rainfall, differences in the antecedent conditions that drive CESM2-LE simulated runoff changes between areas with runoff ratio increases or decreases emerge, largely driven by changes in evapotranspiration via changes in vegetation (Figure 4). As expected, we find a significant difference (Mood's median test) in the medians of antecedent soil water content changes between areas with runoff ratio increase (area-weighted median for soil water change: +0.81%) and areas with decrease (−3.5%). Similarly, we find slight increases in antecedent evapotranspiration associated with decreases in runoff ratio (+0.97%) compared to increases in runoff ratio (−4.6%), where both medians are significantly different from each other (Figure 4b).

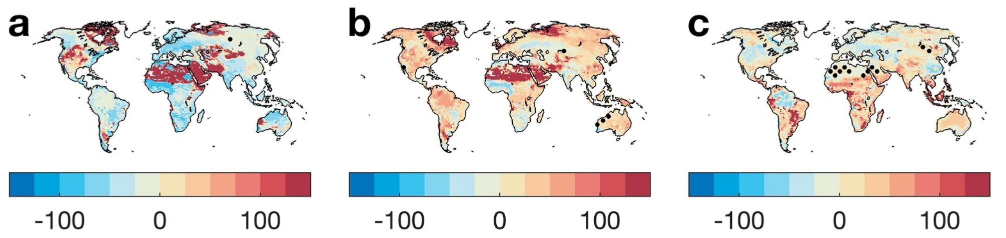

Figure 5. Ensemble mean of percent changes from the historical to projected time period in antecedent (a) transpiration, (b) canopy evaporation, and (c) soil evaporation. The stippling indicates a non-robust (defined as less than 2/3 of the CESM2 large ensemble members agree on sign) increase.

3.4. The Role of Vegetation Greening in Changes in Runoff Ratio and Soil Water Content

To further understand the cause of antecedent evapotranspiration changes and the role of vegetation greening, we now assess changes in individual evapotranspiration components and their relationship to changes in soil water content simulated by the CESM2-LE (Figures 4 and 5). Historically, the approximate area-weighted median of the ratios of antecedent transpiration, antecedent canopy evaporation, and antecedent ground evaporation to total antecedent evapotranspiration are 0.40, 0.20, and 0.40, respectively, though these values can vary significantly depending on vegetation types (or lack of vegetation) and climates. Modeling these individual evapotranspiration components can be highly uncertain, and errors in one component can cascade into errors into the other components (e.g., Miralles et al., 2011; Zhang et al., 2016). It is also important to note that other mechanisms such as changes in roughness, enhanced infiltration from changes in microporosity, and net radiation that are not explicitly assessed in this work can also influence runoff via changes in soil water content and evapotranspiration. Additionally, we find that antecedent VPD, a large driver of evapotranspiration and potential evapotranspiration (Liu et al., 2020) is significantly increasing for much of the global land surface area and likely influences much of the results within this study. However, VPD has large increases in both areas of runoff ratio increases and decreases (Figure 4), suggesting that VPD increases alone are not the sole reason for changes in the runoff ratio. Further, we found essentially no correlation between antecedent canopy evaporation ($r_s = 0.07$), transpiration ($r_s = 0.11$), and a small-to-moderate correlation with antecedent ground evaporation ($r_s = 0.34$) for the entire land surface.

We hypothesize that, via changes in individual evapotranspiration components, projected antecedent greening (increased LAI) leads to a decline in antecedent soil water content that results in a decline in the runoff ratio, even with increases in extreme rainfall. Increased antecedent LAI results in enhanced antecedent transpiration and canopy evaporation, therefore reducing antecedent soil water content (negatively correlated). Further, changes in antecedent soil water content, then, are positively related with antecedent ground evaporation because the declines in antecedent soil water content drive declines in ground evaporation. Building on this, we find strong correlations between antecedent LAI and antecedent transpiration ($r_s = 0.81$) and antecedent LAI and antecedent canopy evaporation ($r_s = 0.63$), and a moderate correlation between antecedent LAI and ground evaporation ($r_s = -0.46$). However, given the complex, non-linear relationships between these variables, we perform a regression tree analysis to understand how projected changes in individual antecedent evapotranspiration components rank in importance in affecting changes in antecedent soil water content.

As before, we analyze the changes in individual CESM2-LE simulated antecedent evapotranspiration components for areas of increases or decreases in runoff ratio and minimal antecedent rainfall change (Figure 4a). We find a clear shift to higher antecedent transpiration for areas with decreases in runoff ratio (land surface median: −12.1%) as compared to areas with increases in runoff ratio (median: −35.9%; Figures 4e and 5), even though antecedent transpiration decreased compared to the historical time period. Using the regression tree models to understand the relative importance of each antecedent evapotranspiration component to changes in antecedent soil water content, we found that antecedent transpiration was the least important evapotranspiration component in determining changes in soil water content in areas of decreased runoff ratios and areas of increased runoff ratios (Figure 6). This indicates, that while changes in antecedent transpiration may be important in dictating changes in antecedent soil water content, changes in the other antecedent evapotranspiration components had a larger effect on changes in antecedent soil water content.

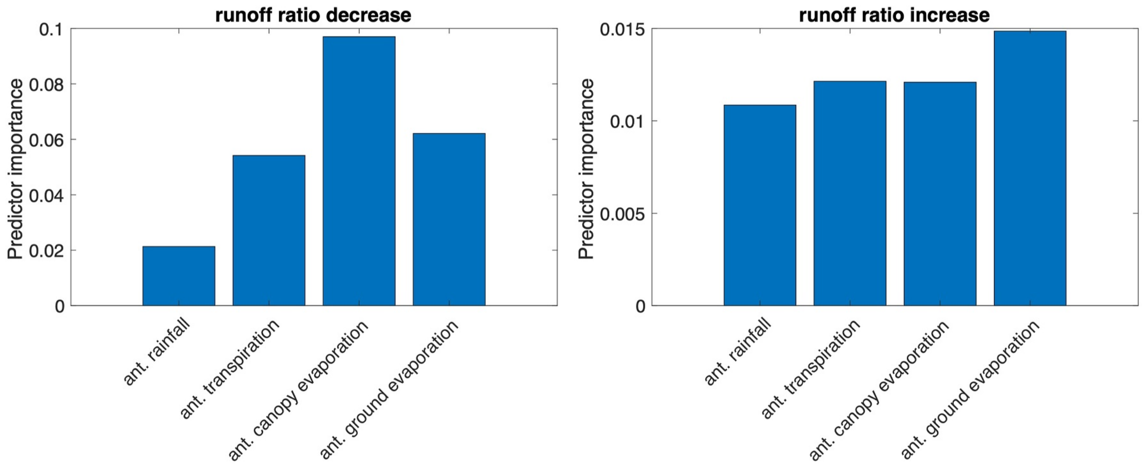

Figure 6. Importance values (defined as an increase in mean square error if the variable is removed divided the sum by the number of branch nodes) for each predictor for areas of runoff ratio increases and areas of runoff ratio decreases.

Projected antecedent transpiration generally declined for both groups compared to the historical time period, even though we find widespread vegetation greening (Zhu et al., 2016; defined here as $LAI_{proj}/LAI_{hist} > 1$; Figure 3c), likely due to a widespread decline in antecedent soil water content (source of evapotranspiration), increased CO_2-induced water-use efficiency (Kooperman et al., 2018; Mankin et al., 2019; Swann et al., 2016; Yang et al., 2019) (average CO_2 for the projected time period is ~780 ppm), and large increases in antecedent VPD for 87% of the land surface (Figures 3d and 4d), further decreasing stomatal conductance and limiting transpiration (Grossiord et al., 2020). However, as previously mentioned, the relationship between LAI_{proj}/LAI_{hist} and change in antecedent transpiration across all land grid cells has a strong positive correlation ($r_s = 0.81$; Figure S27 in Supporting Information S1), suggesting that increased LAI causes transpiration to increase prior to heavy rainfall events (Wang et al., 2014) even though antecedent transpiration itself exhibits projected declines (Figure 4e). Increased LAI and/or earlier leaf-out can also produce warmer conditions (and hence VPD), especially in the northern latitudes (Xu et al., 2020). However, while some differences in the median dates of extreme rainfall event timing (e.g., median day of the year) between areas with an increase or decrease in runoff ratio exist (Figure S28 in Supporting Information S1), the difference is minimal, with a shift in +1.8 days for areas with runoff ratio increases and +2.5 days for areas with runoff ratio decreases (Figure S29 in Supporting Information S1).

While projected antecedent transpiration generally decreases, simulated antecedent canopy evaporation increases for a majority of the land surface (Figure 5), even when controlling for minimal change in antecedent rainfall (Figure 4f). Larger projected increases in canopy evaporation are found for areas with runoff ratio decreases (median: 38.5%) compared to areas with runoff ratio increases (median: 17.9%; Figure 4f). Based on the regression tree models, for areas of runoff ratio decreases, antecedent canopy evaporation was the most important variable in determining changes in antecedent soil water content, while both antecedent canopy evaporation and transpiration were nearly equal in importance in areas of runoff ratio increases (Figure 6). This indicates that in areas of runoff ratio increases, changes in antecedent canopy evaporation have large importance in determining the changes in antecedent soil water content.

Increased LAI can lead to increased annual canopy evaporation due to increased interception (Mankin et al., 2018), but canopy evaporation also has been shown to decline due to less frequent and more intense rainfall events (Lian et al., 2022). While we show increased extreme rainfall and frequency, we also find a strong correlation between antecedent LAI and canopy evaporation across all land grid cells ($r_s = 0.63$). In addition to greening, the widespread increase in evaporative demand from higher VPD (Figure 4d), as well as increased surface roughness from higher LAI values (Xu et al., 2020), would further result in increased canopy evaporation.

In contrast to antecedent canopy evaporation, we find that projected decreases in the simulated runoff ratio are largely associated with slight decreases in antecedent ground evaporation (median = −1.3%; Figures 4g and 5). Increases in runoff ratio, however, are associated with increases in antecedent ground evaporation (median = +18.2%), driven by larger negative shifts in antecedent transpiration and canopy evaporation from an overall lower probability of large antecedent LAI increases (Figure 4c). The regression tree models confirm this, where antecedent ground evaporation is the most important variable in determining changes in antecedent soil water content for areas of runoff ratio increases (Figure 6). With a large increase in LAI, more of the antecedent evapotranspiration would shift to occur via transpiration and canopy evaporation rather than ground evaporation (Mankin et al., 2018; Piao et al., 2020). Our results show this as well, with a moderate negative correlation between changes in antecedent ground evaporation and LAI ($r_s = -0.46$) across all land grid cells, with a stronger correlation in areas of runoff ratio increases ($r_s = -0.58$) than decreases ($r_s = -0.40$). This is further highlighted by a moderate negative correlation between antecedent ground evaporation and canopy evaporation ($r_s = -0.43$) in areas of runoff ratio increases. Additionally, increases in runoff ratio are associated with increases in antecedent soil water content, thus allowing for a larger soil water pool for antecedent ground evaporation to occur if the energy is available (Jung et al., 2010).

4. Summary and Implications

Runoff generation from extreme rainfall is a complex, dynamic mechanism that depends on antecedent conditions and vegetation status. Here, using a prominent and state-of-the-art large climate model ensemble, we shed light on this complexity and show that even with climate-change-induced increases in the magnitude and number of extreme rainfall events, the runoff ratio during these events is projected to decline for the majority of the land surface, in spite of general increases in the amount of runoff. These simulated declines in projected runoff ratio are largely attributed to projected decreases in antecedent soil water content. For areas where the ensemble projects declines in the runoff ratio with minimal changes in antecedent rainfall, the decrease in antecedent soil-water content is associated with vegetation-greening-induced increases in canopy evaporation and increased antecedent atmospheric water demand. Using a machine learning regression tree approach, we find that antecedent canopy evaporation is a key variable associated with projected changes in soil-water content in areas of decreased runoff ratios, which changes in antecedent ground evaporation was the most important variable for areas with increased runoff ratios. Our results suggest that vegetation greening combined with increased evaporative demand will play an important role in the dampening of runoff from extreme rainfall in the future.

While this work uses a large ensemble from a single climate model to understand mechanisms of simulated change in the event rainfall-runoff ratio, the results fall in line with recent empirical work on these mechanisms (Fowler et al., 2022; Trancoso et al., 2017; Ukkola et al., 2016; Williams et al., 2022). Additionally, this work does not specifically examine how land use/land cover change (LULC) might influence the extreme rainfall/runoff relationship. The SSP3 scenario used in this work has a relatively aggressive loss of forest area and natural land, largely replaced by cropland and pastures (O'Neill et al., 2016), which would certainly have an influence on LAI and thus runoff. Even so, given the influence of LULC on hydrology, any impacts from LULC would be reflected in our analysis of LAI and other hydrologic variables.

This work is a first step to understand how climate change may alter the relationship between extreme rain and extreme runoff. Future work should examine whether greening has an influence on the vertical movement of water in the soil column from enhanced interception and increased availability of soil water infiltration. Moving forward, analyses should be performed on remote sensing data sets and sophisticated land surface and climate models that produce the output used in this work at least a daily time step and higher spatial resolution that can address the questions proposed in this work. In summary, planning for the impacts of extreme rainfall events should increasingly consider the responses of vegetation to changing climate and the resultant effect on antecedent soil moisture conditions.

Data Availability Statement

The CESM2-LE output is available at Danabasoglu et al. (2021). The NCEP2 output is available at Kanamitsu et al. (2002b). *Code availability*: Codes used to extract individual rainfall/runoff events and their antecedent conditions can be found at Ficklin (2023).

Acknowledgments

The authors acknowledge the Indiana University Pervasive Technology Institute for providing (supercomputing, visualization, database, storage, and/or consulting) resources that have contributed to the research results reported within this paper. This research was also supported in part by Lilly Endowment, Inc., through its support for the Indiana University Pervasive Technology Institute. D.T. was supported by the National Center for Atmospheric Research, which is a major facility sponsored by the National Science Foundation under Cooperative Agreement No. 1852977, the Walter Scott, Jr. College of Engineering at Colorado State University and the LAD climate group. L.W. acknowledges support from the Division of Earth Sciences (EAR-1554894) and Division of Environmental Biology (DEB-2307257) of the National Science Foundation. We acknowledge the CESM2 Large Ensemble Community Project and supercomputing resources provided by the IBS Center for Climate Physics in South Korea. B.I.C. supported by NASA's Modeling, Analysis, and Prediction program.

References

Abdelmoaty, H. M., Papalexiou, S. M., Rajulapati, C. R., & AghaKouchak, A. (2021). Biases beyond the mean in CMIP6 extreme precipitation: A global investigation. *Earth's Future*, *9*(10), e2021EF002196. https://doi.org/10.1029/2021EF002196

Akinsanola, A., Kooperman, G., Pendergrass, A., Hannah, W., & Reed, K. (2020). Seasonal representation of extreme precipitation indices over the United States in CMIP6 present-day simulations. *Environmental Research Letters*, *15*(9), 094003. https://doi.org/10.1088/1748-9326/ab92c1

Allan, R. P., Hawkins, E., Bellouin, N., & Collins, B. (2021). *IPCC, 2021: Summary for policymakers*. Cambridge University Press.

Allen, M. R., & Ingram, W. J. (2002). Constraints on future changes in climate and the hydrologic cycle. *Nature*, *419*(6903), 224–232. https://doi.org/10.1038/nature01092

Barbero, R., Fowler, H., Lenderink, G., & Blenkinsop, S. (2017). Is the intensification of precipitation extremes with global warming better detected at hourly than daily resolutions? *Geophysical Research Letters*, *44*(2), 974–983. https://doi.org/10.1002/2016gl071917

Barbero, R., Fowler, H. J., Blenkinsop, S., Westra, S., Moron, V., Lewis, E., et al. (2019). A synthesis of hourly and daily precipitation extremes in different climatic regions. *Weather and Climate Extremes*, *26*, 100219. https://doi.org/10.1016/j.wace.2019.100219

Berg, A., & Sheffield, J. (2018). Soil moisture–evapotranspiration coupling in CMIP5 models: Relationship with simulated climate and projections. *Journal of Climate*, *31*(12), 4865–4878. https://doi.org/10.1175/jcli-d-17-0757.1

Berghuijs, W. R., Harrigan, S., Molnar, P., Slater, L. J., & Kirchner, J. W. (2019). The relative importance of different flood-generating mechanisms across Europe. *Water Resources Research*, *55*(6), 4582–4593. https://doi.org/10.1029/2019WR024841

Blöschl, G., Hall, J., Viglione, A., Perdigão, R. A. P., Parajka, J., Merz, B., et al. (2019). Changing climate both increases and decreases European river floods. *Nature*, *573*(7772), 108–111. https://doi.org/10.1038/s41586-019-1495-6

Breiman, L. (1996). Bagging predictors. *Machine Learning*, *24*(2), 123–140. https://doi.org/10.1007/bf00058655

Breiman, L. (2001). Random forests. *Machine Learning*, *45*(1), 5–32. https://doi.org/10.1023/a:1010933404324

Brocca, L., Melone, F., & Moramarco, T. (2008). On the estimation of antecedent wetness conditions in rainfall–runoff modelling. *Hydrological Processes*, *22*(5), 629–642. https://doi.org/10.1002/hyp.6629

Burn, D. H., & Whitfield, P. H. (2023). Climate related changes to flood regimes show an increasing rainfall influence. *Journal of Hydrology*, *617*, 129075. https://doi.org/10.1016/j.jhydrol.2023.129075

Claverie, M., Matthews, J. L., Vermote, E. F., & Justice, C. O. (2016). A 30+ Year AVHRR LAI and FAPAR climate data record: Algorithm description and validation. *Remote Sensing*, *8*(3), 263. https://doi.org/10.3390/rs8030263

Collier, N., Hoffman, F. M., Lawrence, D. M., Keppel-Aleks, G., Koven, C. D., Riley, W. J., et al. (2018). The International Land Model Benchmarking (ILAMB) system: Design, theory, and implementation. *Journal of Advances in Modeling Earth Systems*, *10*(11), 2731–2754. https://doi.org/10.1029/2018MS001354

Cook, B. I., Mankin, J. S., Marvel, K., Williams, A. P., Smerdon, J. E., & Anchukaitis, K. J. (2020). Twenty-first century drought projections in the CMIP6 forcing scenarios. *Earth's Future*, *8*(6), e2019EF001461. https://doi.org/10.1029/2019EF001461

Danabasoglu, G., Deser, K. B., Rodgers, C., & Timmermann, A. (2021). CESM2 large ensemble [Dataset]. *Climate Data Gateway*. https://doi.org/10.26024/kgmp-c556

Danabasoglu, G., Lamarque, J.-F., Bacmeister, J., Bailey, D. A., DuVivier, A. K., Edwards, J., et al. (2020). The Community Earth System Model Version 2 (CESM2). *Journal of Advances in Modeling Earth Systems*, *12*(2), e2019MS001916. https://doi.org/10.1029/2019MS001916

Feng, Y., Wang, H., Liu, W., & Sun, F. (2023). Global soil moisture–climate interactions during the peak growing season. *Journal of Climate*, *36*(4), 1187–1196. https://doi.org/10.1175/jcli-d-22-0161.1

Ficklin, D. L. (2023). [Software]. *Zenodo*. https://doi.org/10.5281/zenodo.8014783

Ficklin, D. L., & Novick, K. A. (2017). Historic and projected changes in vapor pressure deficit suggest a continental-scale drying of the United States atmosphere. *Journal of Geophysical Research: Atmospheres*, *122*(4), 2061–2079. https://doi.org/10.1002/2016JD025855

Ficklin, D. L., Null, S. E., Abatzoglou, J. T., Novick, K. A., & Myers, D. T. (2022). Hydrological intensification will increase the complexity of water resource management. *Earth's Future*, *10*(3), e2021EF002487. https://doi.org/10.1029/2021ef002487

Fowler, K., Peel, M., Saft, M., Peterson, T. J., Western, A., Band, L., et al. (2022). Explaining changes in rainfall–runoff relationships during and after Australia's Millennium drought: A community perspective. *Hydrology and Earth System Sciences*, *26*(23), 6073–6120. https://doi.org/10.5194/hess-26-6073-2022

Gelman, A., & Stern, H. (2006). The difference between "significant" and "not significant" is not itself statistically significant. *The American Statistician*, *60*(4), 328–331. https://doi.org/10.1198/000313006X152649

Gillett, N. P., Cannon, A. J., Malinina, E., Schnorbus, M., Anslow, F., Sun, Q., et al. (2022). Human influence on the 2021 British Columbia floods. *Weather and Climate Extremes*, *36*, 100441. https://doi.org/10.1016/j.wace.2022.100441

Grossiord, C., Buckley, T. N., Cernusak, L. A., Novick, K. A., Poulter, B., Siegwolf, R. T. W., et al. (2020). Plant responses to rising vapor pressure deficit. *New Phytologist*, *226*(6), 1550–1566. https://doi.org/10.1111/nph.16485

Halsey, L. G. (2019). The reign of the p-value is over: What alternative analyses could we employ to fill the Power Vacuum? *Biology Letters*, *15*(5), 20190174. https://doi.org/10.1098/rsbl.2019.0174

Hobeichi, S., Abramowitz, G., & Evans, J. (2020). Conserving Land–Atmosphere Synthesis Suite (CLASS). *Journal of Climate*, *33*(5), 1821–1844. https://doi.org/10.1175/jcli-d-19-0036.1

Hobeichi, S., Abramowitz, G., Evans, J., & Beck, H. E. (2019). Linear Optimal Runoff Aggregate (LORA): A global gridded synthesis runoff product. *Hydrology and Earth System Sciences*, *23*(2), 851–870. https://doi.org/10.5194/hess-23-851-2019

Ivancic, T. J., & Shaw, S. B. (2015). Examining why trends in very heavy precipitation should not be mistaken for trends in very high river discharge. *Climatic Change*, *133*(4), 681–693. https://doi.org/10.1007/s10584-015-1476-1

James, G., Witten, D., Hastie, T., & Tibshirani, R. (2013). *An introduction to statistical learning 112*. Springer. 18.

Jung, M., Reichstein, M., Ciais, P., Seneviratne, S. I., Sheffield, J., Goulden, M. L., et al. (2010). Recent decline in the global land evapotranspiration trend due to limited moisture supply. *Nature*, *467*(7318), 951–954. https://doi.org/10.1038/nature09396

Kanamitsu, M., Ebisuzaki, W., Woollen, J., Yang, S. K., Hnilo, J. J., Fiorino, M., & Potter, G. L. (2002a). NCEP–DOE AMIP-II reanalysis (r-2). *Bulletin of the American Meteorological Society*, *83*(11), 1631–1644. https://doi.org/10.1175/bams-83-11-1631(2002)083<1631:nar>2.3.co;2

Kanamitsu, M., Ebisuzaki, W., Woollen, J., Yang, S. K., Hnilo, J. J., Fiorino, M., & Potter, G. L. (2002b). National Centers for environmental prediction/department of energy reanalysis II [Dataset]. https://psl.noaa.gov/data/gridded/data.ncep.reanalysis2.html

Katsuyama, M., Kabeya, N., & Ohte, N. (2009). Elucidation of the relationship between geographic and time sources of stream water using a tracer approach in a headwater catchment. *Water Resources Research*, *45*(6). https://doi.org/10.1029/2008WR007458

Kirchmeier-Young, M. C., & Zhang, X. (2020). Human influence has intensified extreme precipitation in North America. *Proceedings of the National Academy of Sciences*, *117*(24), 13308–13313. https://doi.org/10.1073/pnas.1921628117

Kooperman, G. J., Fowler, M. D., Hoffman, F. M., Koven, C. D., Lindsay, K., Pritchard, M. S., et al. (2018). Plant physiological responses to rising CO_2 modify simulated daily runoff intensity with implications for global-scale flood risk assessment. *Geophysical Research Letters*, *45*(22), 12457–412466. https://doi.org/10.1029/2018GL079901

Lawrence, D. M., Fisher, R. A., Koven, C. D., Oleson, K. W., Swenson, S. C., Bonan, G., et al. (2019). The community land model version 5: Description of new features, benchmarking, and impact of forcing uncertainty. *Journal of Advances in Modeling Earth Systems*, *11*(12), 4245–4287. https://doi.org/10.1029/2018MS001583

Li, Y., Zhang, W., Schwalm, C. R., Gentine, P., Smith, W. K., Ciais, P., et al. (2023). Widespread spring phenology effects on drought recovery of Northern Hemisphere ecosystems. *Nature Climate Change*, *13*(2), 182–188. https://doi.org/10.1038/s41558-022-01584-2

Lian, X., Zhao, W., & Gentine, P. (2022). Recent global decline in rainfall interception loss due to altered rainfall regimes. *Nature Communications*, *13*(1), 7642. https://doi.org/10.1038/s41467-022-35414-y

Liu, X., Li, C., Zhao, T., & Han, L. (2020). Future changes of global potential evapotranspiration simulated from CMIP5 to CMIP6 models. *Atmospheric and Oceanic Science Letters*, *13*(6), 568–575. https://doi.org/10.1080/16742834.2020.1824983

Mallakpour, I., & Villarini, G. (2015). The changing nature of flooding across the central United States. *Nature Climate Change*, *5*(3), 250–254. https://doi.org/10.1038/nclimate2516

Mankin, J. S., Lehner, F., Coats, S., & McKinnon, K. A. (2020). The value of initial condition large ensembles to robust adaptation decision-making. *Earth's Future*, *8*(10), e2012EF001610. https://doi.org/10.1029/2020EF001610

Mankin, J. S., Seager, R., Smerdon, J. E., Cook, B. I., & Williams, A. P. (2019). Mid-latitude freshwater availability reduced by projected vegetation responses to climate change. *Nature Geoscience*, *12*(12), 983–988. https://doi.org/10.1038/s41561-019-0480-x

Mankin, J. S., Seager, R., Smerdon, J. E., Cook, B. I., Williams, A. P., & Horton, R. M. (2018). Blue water trade-offs with vegetation in a CO_2-enriched climate. *Geophysical Research Letters*, *45*(7), 3115–3125. https://doi.org/10.1002/2018GL077051

Mankin, J. S., Smerdon, J. E., Cook, B. I., Williams, A. P., & Seager, R. (2017). The curious case of projected twenty-first-century drying but greening in the American west. *Journal of Climate*, *30*(21), 8689–8710. https://doi.org/10.1175/jcli-d-17-0213.1

Martens, B., Miralles, D. G., Lievens, H., van der Schalie, R., de Jeu, R. A. M., Fernández-Prieto, D., et al. (2017). GLEAM v3: Satellite-based land evaporation and root-zone soil moisture. *Geoscientific Model Development*, *10*(5), 1903–1925. https://doi.org/10.5194/gmd-10-1903-2017

Masson-Delmotte, V., Zhai, P., Pirani, A., Connors, S. L., Péan, C., Berger, S., & Zhou, B. (2021). *Climate change 2021: The physical science basis. Contribution of working group I to the sixth assessment report of the intergovernmental panel on climate change*. Cambridge University Press.

McKinnon, K. A., & Simpson, I. R. (2022). How unexpected was the 2021 pacific Northwest heatwave? *Geophysical Research Letters*, *49*(18), e2022GL100380. https://doi.org/10.1029/2022GL100380

Meinshausen, M., Nicholls, Z. R. J., Lewis, J., Gidden, M. J., Vogel, E., Freund, M., et al. (2020). The Shared Socio-Economic Pathway (SSP) greenhouse gas concentrations and their extensions to 2500. *Geoscientific Model Development*, *13*(8), 3571–3605. https://doi.org/10.5194/gmd-13-3571-2020

Milinski, S., Maher, N., & Olonscheck, D. (2020). How large does a large ensemble need to be? *Earth System Dynamics*, *11*(4), 885–901. https://doi.org/10.5194/esd-11-885-2020

Miralles, D. G., De Jeu, R. A. M., Gash, J. H., Holmes, T. R. H., & Dolman, A. J. (2011). Magnitude and variability of land evaporation and its components at the global scale. *Hydrology and Earth System Sciences*, *15*(3), 967–981. https://doi.org/10.5194/hess-15-967-2011

Mishra, S. K., & Singh, V. P. (2006). A relook at NEH-4 curve number data and antecedent moisture condition criteria. *Hydrological Processes*, *20*(13), 2755–2768. https://doi.org/10.1002/hyp.6066

Mu, Q., Zhao, M., & Running, S. W. (2011). Improvements to a MODIS global terrestrial evapotranspiration algorithm. *Remote Sensing of Environment*, *115*(8), 1781–1800. https://doi.org/10.1016/j.rse.2011.02.019

Musselman, K. N., Lehner, F., Ikeda, K., Clark, M. P., Prein, A. F., Liu, C., et al. (2018). Projected increases and shifts in rain-on-snow flood risk over Western North America. *Nature Climate Change*, *8*(9), 808–812. https://doi.org/10.1038/s41558-018-0236-4

Myneni, R. B., Hoffman, S., Knyazikhin, Y., Privette, J. L., Glassy, J., Tian, Y., et al. (2002). Global products of vegetation leaf area and fraction absorbed PAR from year one of MODIS data. *Remote Sensing of Environment*, *83*(1), 214–231. https://doi.org/10.1016/s0034-4257(02)00074-3

Novick, K. A., Ficklin, D. L., Stoy, P. C., Williams, C. A., Bohrer, G., Oishi, A. C., et al. (2016). The increasing importance of atmospheric demand for ecosystem water and carbon fluxes. *Nature Climate Change*, *6*(11), 1023–1027. https://doi.org/10.1038/nclimate3114

NRCS. (2004). *National engineering handbook: Part 630—hydrology* (pp. 11–15). USDA Soil Conservation Service.

O'Neill, B. C., Tebaldi, C., Van Vuuren, D. P., Eyring, V., Friedlingstein, P., Hurtt, G., et al. (2016). The Scenario Model Intercomparison Project (ScenarioMIP) for CMIP6. *Geoscientific Model Development*, *9*(9), 3461–3482. https://doi.org/10.5194/gmd-9-3461-2016

Pendergrass, A. G. (2018). What precipitation is extreme? *Science*, *360*(6393), 1072–1073. https://doi.org/10.1126/science.aat1871

Pendergrass, A. G., & Knutti, R. (2018). The uneven nature of daily precipitation and its change. *Geophysical Research Letters*, *45*(21), 11980–911988. https://doi.org/10.1029/2018GL080298

Pendergrass, A. G., Meehl, G. A., Pulwarty, R., Hobbins, M., Hoell, A., AghaKouchak, A., et al. (2020). Flash droughts present a new challenge for subseasonal-to-seasonal prediction. *Nature Climate Change*, *10*(3), 191–199. https://doi.org/10.1038/s41558-020-0709-0

Penna, D., Tromp-van Meerveld, H. J., Gobbi, A., Borga, M., & Dalla Fontana, G. (2011). The influence of soil moisture on threshold runoff generation processes in an alpine headwater catchment. *Hydrology and Earth System Sciences*, *15*(3), 689–702. https://doi.org/10.5194/hess-15-689-2011

Piao, S., Wang, X., Park, T., Chen, C., Lian, X., He, Y., et al. (2020). Characteristics, drivers and feedbacks of global greening. *Nature Reviews Earth & Environment*, *1*(1), 14–27. https://doi.org/10.1038/s43017-019-0001-x

Polson, D., Hegerl, G. C., Zhang, X., & Osborn, T. J. (2013). Causes of robust seasonal land precipitation changes. *Journal of Climate*, *26*(17), 6679–6697. https://doi.org/10.1175/jcli-d-12-00474.1

Rodgers, K. B., Lee, S. S., Rosenbloom, N., Timmermann, A., Danabasoglu, G., Deser, C., et al. (2021). Ubiquity of human-induced changes in climate variability. *Earth System Dynamics Discuss*, *2021*(4), 1–22. https://doi.org/10.5194/esd-12-1393-2021

Scheff, J., Coats, S., & Laguë, M. M. (2022). Why do the global warming responses of land-surface models and climatic dryness metrics disagree? *Earth's Future*, *10*(8), e2022EF002814. https://doi.org/10.1029/2022EF002814

Scipal, K., Scheffler, C., & Wagner, W. (2005). Soil moisture-runoff relation at the catchment scale as observed with coarse resolution microwave remote sensing. *Hydrology and Earth System Sciences*, *9*(3), 173–183. https://doi.org/10.5194/hess-9-173-2005

Sharma, A., Wasko, C., & Lettenmaier, D. P. (2018). If precipitation extremes are increasing, why aren't floods? *Water Resources Research*, *54*(11), 8545–8551. https://doi.org/10.1029/2018wr023749

Singh, N. K., Emanuel, R. E., McGlynn, B. L., & Miniat, C. F. (2021). Soil moisture responses to rainfall: Implications for runoff generation. *Water Resources Research*, *57*(9), e2020WR028827. https://doi.org/10.1029/2020WR028827

Stevenson, S., Coats, S., Touma, D., Cole, J., Lehner, F., Fasullo, J., & Otto-Bliesner, B. (2022). Twenty-first century hydroclimate: A continually changing baseline, with more frequent extremes. *Proceedings of the National Academy of Sciences*, *119*(12), e2108124119. https://doi.org/10.1073/pnas.2108124119

Swann, A. L. S., Hoffman, F. M., Koven, C. D., & Randerson, J. T. (2016). Plant responses to increasing CO_2 reduce estimates of climate impacts on drought severity. *Proceedings of the National Academy of Sciences*, *113*(36), 10019–10024. https://doi.org/10.1073/pnas.1604581113

Touma, D., Stevenson, S., Lehner, F., & Coats, S. (2021). Human-driven greenhouse gas and aerosol emissions cause distinct regional impacts on extreme fire weather. *Nature Communications*, *12*(1), 212. https://doi.org/10.1038/s41467-020-20570-w

Touma, D., Stevenson, S., Swain, D. L., Singh, D., Kalashnikov, D. A., & Huang, X. (2022). Climate change increases risk of extreme rainfall following wildfire in the Western United States. *Science Advances*, *8*(13), eabm0320. https://doi.org/10.1126/sciadv.abm0320

Trancoso, R., Larsen, J. R., McVicar, T. R., Phinn, S. R., & McAlpine, C. A. (2017). CO_2-vegetation feedbacks and other climate changes implicated in reducing base flow. *Geophysical Research Letters*, *44*(5), 2310–2318. https://doi.org/10.1002/2017GL072759

Ukkola, A. M., Prentice, I. C., Keenan, T. F., van Dijk, A. I. J. M., Viney, N. R., Myneni, R. B., & Bi, J. (2016). Reduced streamflow in water-stressed climates consistent with CO_2 effects on vegetation. *Nature Climate Change*, *6*(1), 75–78. https://doi.org/10.1038/nclimate2831

Vermote, E. (2019). *NOAA Climate Data Record (CDR) of AVHRR leaf area index (LAI) and Fraction of Absorbed Photosynthetically Active Radiation (FAPAR), version 5*. NOAA National Centers for Environmental Information.

Visser, J. B., Wasko, C., Sharma, A., & Nathan, R. (2021). Eliminating the "hook" in precipitation–temperature scaling. *Journal of Climate*, *34*(23), 9535–9549.

Wang, L., Good, S. P., & Caylor, K. K. (2014). Global synthesis of vegetation control on evapotranspiration partitioning. *Geophysical Research Letters*, *41*(19), 6753–6757. https://doi.org/10.1002/2014GL061439

Wang, Y., Mao, J., Jin, M., Hoffman, F. M., Shi, X., Wullschleger, S. D., & Dai, Y. (2021). Development of observation-based global multilayer soil moisture products for 1970 to 2016. *Earth System Science Data*, *13*(9), 4385–4405. https://doi.org/10.5194/essd-13-4385-2021

Wasko, C., & Nathan, R. (2019). Influence of changes in rainfall and soil moisture on trends in flooding. *Journal of Hydrology*, *575*, 432–441. https://doi.org/10.1016/j.jhydrol.2019.05.054

Wasko, C., Nathan, R., Stein, L., & O'Shea, D. (2021). Evidence of shorter more extreme rainfalls and increased flood variability under climate change. *Journal of Hydrology*, *603*, 126994. https://doi.org/10.1016/j.jhydrol.2021.126994

Westra, S., Alexander, L. V., & Zwiers, F. W. (2013). Global increasing trends in annual maximum daily precipitation. *Journal of Climate*, *26*(11), 3904–3918. https://doi.org/10.1175/jcli-d-12-00502.1

Wieder, W. R., Kennedy, D., Lehner, F., Musselman, K. N., Rodgers, K. B., Rosenbloom, N., et al. (2022). Pervasive alterations to snow-dominated ecosystem functions under climate change. *Proceedings of the National Academy of Sciences*, *119*(30), e2202393119. https://doi.org/10.1073/pnas.2202393119

Williams, A. P., Livneh, B., McKinnon, K. A., Hansen, W. D., Mankin, J. S., Cook, B. I., et al. (2022). Growing impact of wildfire on western US water supply. *Proceedings of the National Academy of Sciences*, *119*(10), e2114069119. https://doi.org/10.1073/pnas.2114069119

Willmott, C. J., Robeson, S. M., & Matsuura, K. (2007). Geographic box plots. *Physical Geography*, *28*(4), 331–344. https://doi.org/10.2747/0272-3646.28.4.331

Woldemeskel, F., & Sharma, A. (2016). Should flood regimes change in a warming climate? The role of antecedent moisture conditions. *Geophysical Research Letters*, *43*(14), 7556–7563. https://doi.org/10.1002/2016GL069448

Xu, X., Riley, W. J., Koven, C. D., Jia, G., & Zhang, X. (2020). Earlier leaf-out warms air in the north. *Nature Climate Change*, *10*(4), 370–375. https://doi.org/10.1038/s41558-020-0713-4

Yang, Y., Roderick, M. L., Zhang, S., McVicar, T. R., & Donohue, R. J. (2019). Hydrologic implications of vegetation response to elevated CO_2 in climate projections. *Nature Climate Change*, *9*(1), 44–48. https://doi.org/10.1038/s41558-018-0361-0

Yuan, X., Wang, Y., Ji, P., Wu, P., Sheffield, J., & Otkin, J. A. (2023). A global transition to flash droughts under climate change. *Science*, *380*(6641), 187–191. https://doi.org/10.1126/science.abn6301

Zeder, J., & Fischer, E. M. (2024). Decadal to centennial extreme precipitation disaster gaps — Long-term variability and implications for extreme value modelling. *Weather and Climate Extremes*, *43*, 100636. https://doi.org/10.1016/j.wace.2023.100636

Zhang, S., Zhou, L., Zhang, L., Yang, Y., Wei, Z., Zhou, S., et al. (2022). Reconciling disagreement on global river flood changes in a warming climate. *Nature Climate Change*, *12*(12), 1160–1167. https://doi.org/10.1038/s41558-022-01539-7

Zhang, Y., Chiew, F. H., Li, M., & Post, D. (2018). Predicting runoff signatures using regression and hydrological modeling approaches. *Water Resources Research*, *54*(10), 7859–7878. https://doi.org/10.1029/2018wr023325

Zhang, Y., Peña-Arancibia, J. L., McVicar, T. R., Chiew, F. H., Vaze, J., Liu, C., et al. (2016). Multi-decadal trends in global terrestrial evapotranspiration and its components. *Scientific Reports*, *6*(1), 19124. https://doi.org/10.1038/srep19124

Zhu, Z., Piao, S., Myneni, R. B., Huang, M., Zeng, Z., Canadell, J. G., et al. (2016). Greening of the Earth and its drivers. *Nature Climate Change*, *6*(8), 791–795. https://doi.org/10.1038/nclimate3004

References From the Supporting Information

Bi, D., Dix, M., Marsland, S., O'Farrell, S., Sullivan, A., Bodman, R., et al. (2020). Configuration and spin-up of ACCESS-CM2, the new generation Australian community climate and Earth system simulator coupled model. *Journal of Southern Hemisphere Earth Systems Science*, *70*(1), 225–251. https://www.publish.csiro.au/paper/ES19040

Boucher, O., Denvil, S., Levavasseur, G., Cozic, A., Caubel, A., Foujols, M.-A., et al. (2018). IPSL IPSL-CM6A-LR model output prepared for CMIP6 CMIP. https://doi.org/10.22033/ESGF/CMIP6.1534

Cherchi, A., Fogli, P. G., Lovato, T., Peano, D., Iovino, D., Gualdi, S., et al. (2019). Global mean climate and main patterns of variability in the CMCC-CM2 coupled model. *Journal of Advances in Modeling Earth Systems*, *11*(1), 185–209. https://doi.org/10.1029/2018MS001369

Fang, H., Baret, F., Plummer, S., & Schaepman-Strub, G. (2019). An overview of global Leaf Area Index (LAI): Methods, products, validation, and applications. *Reviews of Geophysics*, *57*(3), 739–799. https://doi.org/10.1029/2018RG000608

Gray, L. C., Zhao, L., & Stillwell, A. S. (2023). Impacts of climate change on global total and urban runoff. *Journal of Hydrology*, *620*, 129352. https://doi.org/10.1016/j.jhydrol.2023.129352

He, B., Bao, Q., Wang, X., Zhou, L., Wu, X., Liu, Y., et al. (2019). CAS FGOALS-f3-L model datasets for CMIP6 historical atmospheric model intercomparison project simulation. *Advances in Atmospheric Sciences*, *36*(8), 771–778. https://doi.org/10.1007/s00376-019-9027-8

Kay, A. L., Davies, H. N., Bell, V. A., & Jones, R. G. (2009). Comparison of uncertainty sources for climate change impacts: Flood frequency in England. *Climatic Change*, *92*(1–2), 41–63. https://doi.org/10.1007/s10584-10008-19471-10584

Krasting, J. P., John, J. G., Blanton, C., McHugh, C., Nikonov, S., Radhakrishnan, A., et al. (2018). NOAA-GFDL GFDL-ESM4 model output prepared for CMIP6 CMIP historical. https://doi.org/10.22033/ESGF/CMIP6.8597

Li, X., Melaas, E., Carrillo, C. M., Ault, T., Richardson, A. D., Lawrence, P., et al. (2022). A comparison of land surface phenology in the northern hemisphere derived from satellite remote sensing and the community land model. *Journal of Hydrometeorology*, *23*(6), 859–873. https://doi.org/10.1175/jhm-d-21-0169.1

Liang, X., Lettenmaier, D. P., Wood, E. F., & Burges, S. J. (1994). A simple hydrologically based model of land surface water and energy fluxes for general circulation models. *Journal of Geophysical Research*, *99*(D7), 14415–14428. https://doi.org/10.1029/94jd00483

Livneh, B., Rosenberg, E. A., Lin, C., Nijssen, B., Mishra, V., Andreadis, K. M., et al. (2013). A long-term hydrologically based dataset of land surface fluxes and states for the conterminous United States: Update and extensions. *Journal of Climate*, *26*(23), 9384–9392. https://doi.org/10.1175/jcli-d-12-00508.1

Mauritsen, T., Bader, J., Becker, T., Behrens, J., Bittner, M., Brokopf, R., et al. (2019). Developments in the MPI-M Earth System Model Version 1.2 (MPI-ESM1.2) and its response to increasing CO_2. *Journal of Advances in Modeling Earth Systems*, *11*(4), 998–1038. https://doi.org/10.1029/2018MS001400

Oleson, K. W., Niu, G.-Y., Yang, Z.-L., Lawrence, D. M., Thornton, P. E., Lawrence, P. J., et al. (2008). Improvements to the Community Land Model and their impact on the hydrological cycle. *Journal of Geophysical Research*, *113*(G1). https://doi.org/10.1029/2007JG000563

Park, H., & Jeong, S. (2021). Leaf area index in Earth system models: How the key variable of vegetation seasonality works in climate projections. *Environmental Research Letters*, *16*(3), 034027. https://doi.org/10.1088/1748-9326/abe2cf

Seland, Ø., Bentsen, M., Olivié, D., Toniazzo, T., Gjermundsen, A., Graff, L. S., et al. (2020). Overview of the Norwegian Earth System Model (NorESM2) and key climate response of CMIP6 DECK, historical, and scenario simulations. *Geoscientific Model Development*, *13*(12), 6165–6200. https://doi.org/10.5194/gmd-13-6165-2020

Swart, N. C., Cole, J. N. S., Kharin, V. V., Lazare, M., Scinocca, J. F., Gillett, N. P., et al. (2019). The Canadian Earth System Model Version 5 (CanESM5.0.3). *Geoscientific Model Development*, *12*(11), 4823–4873. https://doi.org/10.5194/gmd-12-4823-2019

Tatebe, H., & Watanabe, M. (2018). MIROC MIROC6 model output prepared for CMIP6 CMIP. https://doi.org/10.22033/ESGF/CMIP6.881

Tye, M. R., Ge, M., Richter, J. H., Gutmann, E. D., Rugg, A., Bruyère, C. L., & Wood, A. (2023). *Evaluating an Earth system model from a water user perspective* (Vol. 2023, pp. 1–33). EGUsphere.

Volodin, E., & Gritsun, A. (2018). Simulation of observed climate changes in 1850–2014 with climate model INM-CM5. *Earth System Dynamics*, *9*(4), 1235–1242. https://doi.org/10.5194/esd-9-1235-2018

Willmott, C. J., Robeson, S. M., & Matsuura, K. (2012). A refined index of model performance. *International Journal of Climatology*, *32*(13), 2088–2094. https://doi.org/10.1002/joc.2419

Wu, T., Lu, Y., Fang, Y., Xin, X., Li, L., Li, W., et al. (2019). The Beijing Climate Center Climate System Model (BCC-CSM): The main progress from CMIP5 to CMIP6. *Geoscientific Model Development*, *12*(4), 1573–1600. https://doi.org/10.5194/gmd-12-1573-2019

Yukimoto, S., Kawai, H., Koshiro, T., Oshima, N., Yoshida, K., Urakawa, S., et al. (2019). The meteorological research Institute Earth system model version 2.0, MRI-ESM2. 0: Description and basic evaluation of the physical component. *Journal of the Meteorological Society of Japan. Ser. II*, *97*(5), 931–965. https://doi.org/10.2151/jmsj.2019-051

Zhang, H., Zhang, M., Jin, J., Fei, K., Ji, D., Wu, C., et al. (2020). Description and climate simulation performance of CAS-ESM version 2. *Journal of Advances in Modeling Earth Systems*, *12*(12), e2020MS002210. https://doi.org/10.1029/2020MS002210

Ziehn, T., Chamberlain, M. A., Law, R. M., Lenton, A., Bodman, R. W., Dix, M., et al. (2020). The Australian Earth system model: ACCESS-ESM1.5. *Journal of Southern Hemisphere Earth Systems Science*, *70*(1), 193–214. https://www.publish.csiro.au/paper/ES19035